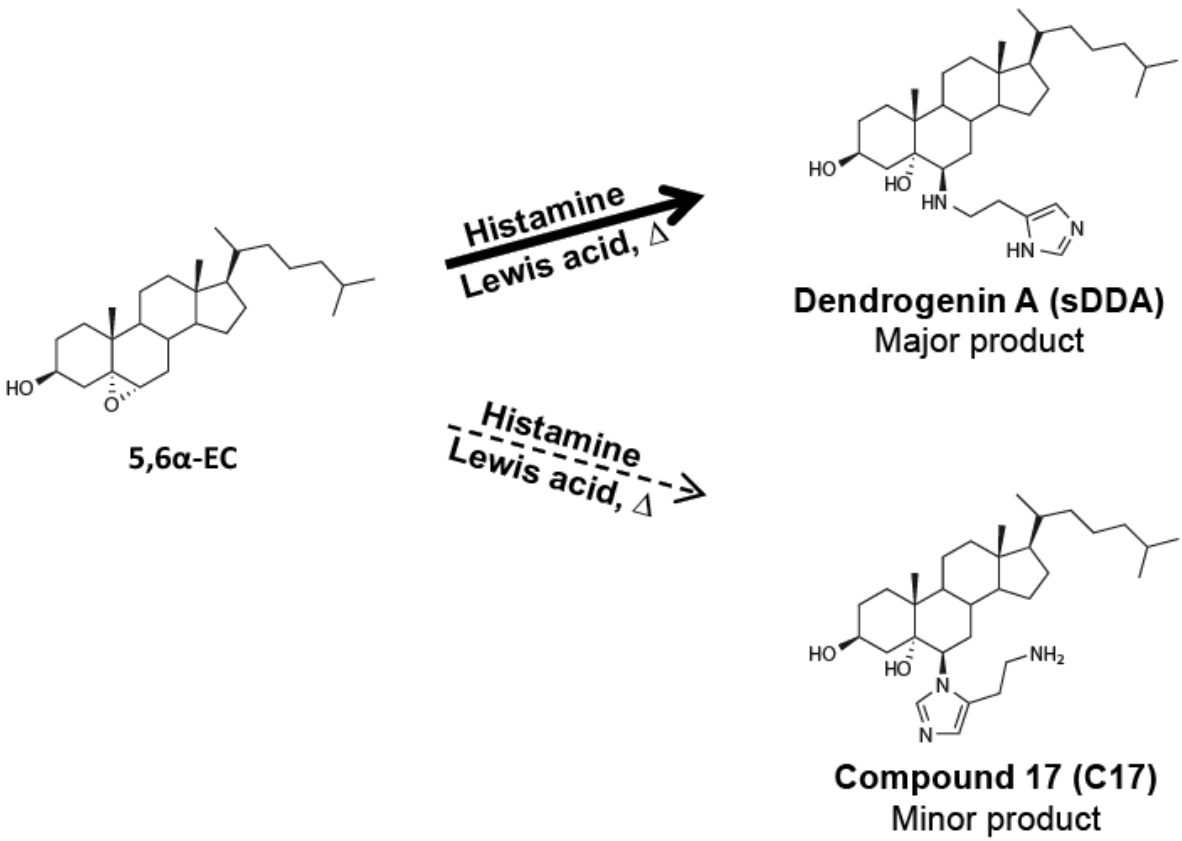

Supplementary Figure S1 | Scheme describing the chemical synthesis of DDA under catalytic conditions. The reaction of 5,6α-EC with histamine was possible in the presence of a catalyst to give DDA as the major product and C17 as a minor product [21].

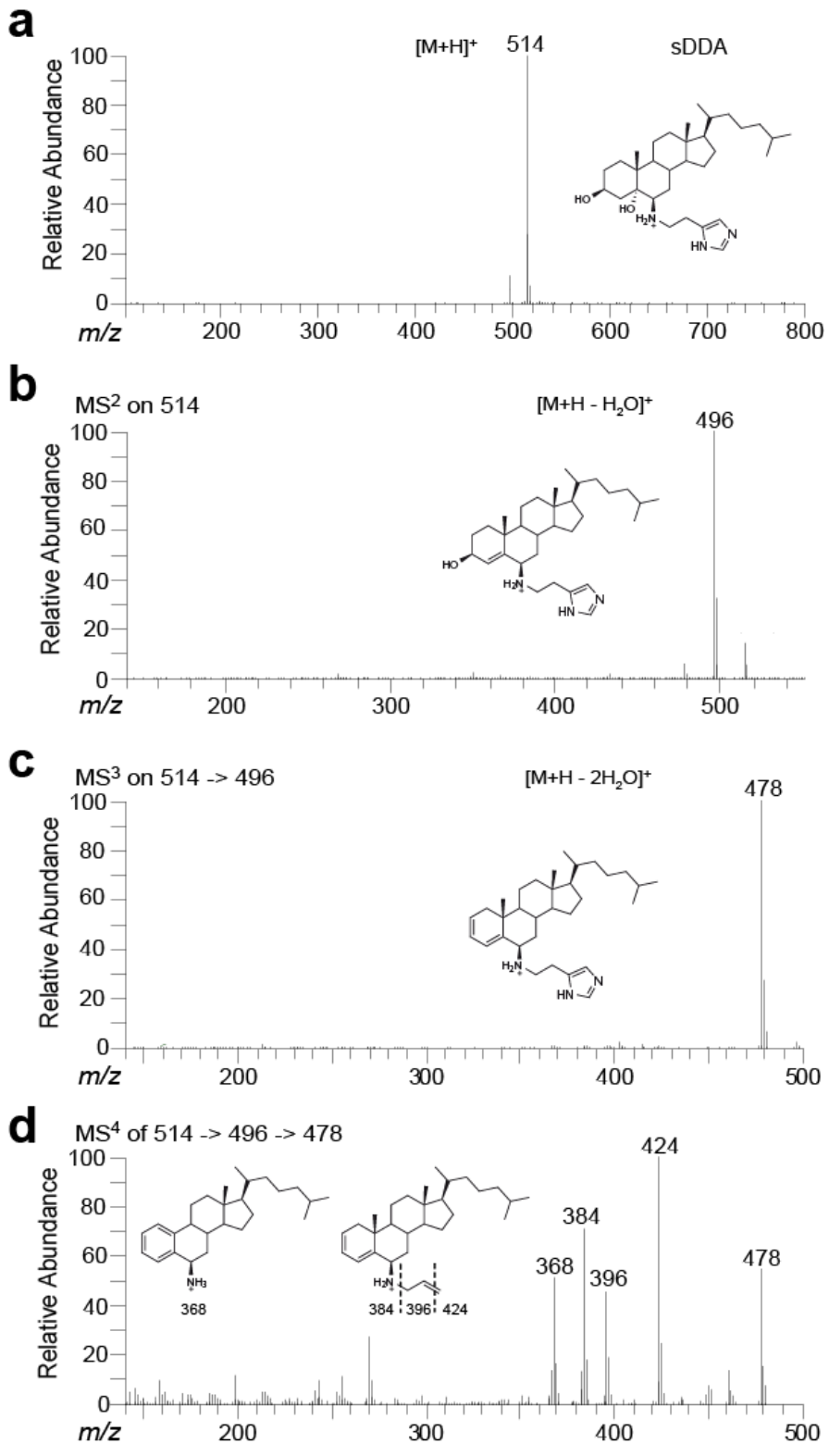

Supplementary Figure S2 | NanoESI fragmentation of synthetic DDA (sDDA). (a) NanoESI Mass spectrometry fragmentation (MS^1) profile of sDDA and chemical structure of sDDA. (b) MS^2 fragmentation of the $[M+H]^+$ (*m/z* 514) peak obtained in MS^1. (c) MS^3 fragmentation of the (*m/z* 496) peak obtained in MS^2. (d) MS^4 fragmentation of the (*m/z* 478) peak obtained in MS^3.

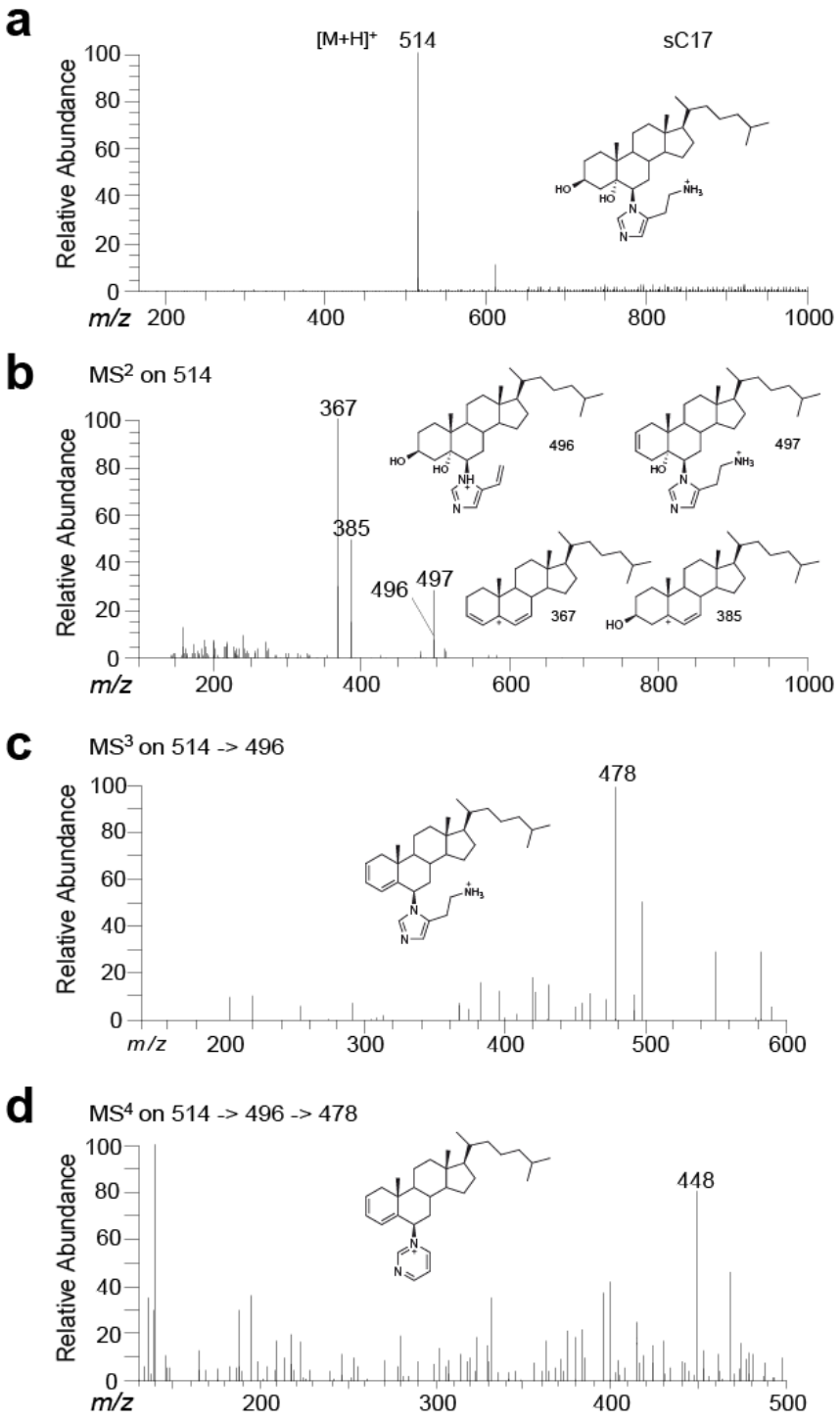

Supplementary Figure S3 | NanoESI fragmentation profiles of synthetic C17 (sC17). (a) nanoESI Mass spectrometry fragmentation (MS^1) profile of C17 and chemical structure of C17. (b) MS^2 fragmentation of the $[M+H]^+$ (*m/z* 514) peak obtained in MS^1. (c) MS^3 fragmentation of the (*m/z* 496) peak obtained in MS^2. (d) MS^4 fragmentation of the (*m/z* 478) peak obtained in MS^3.

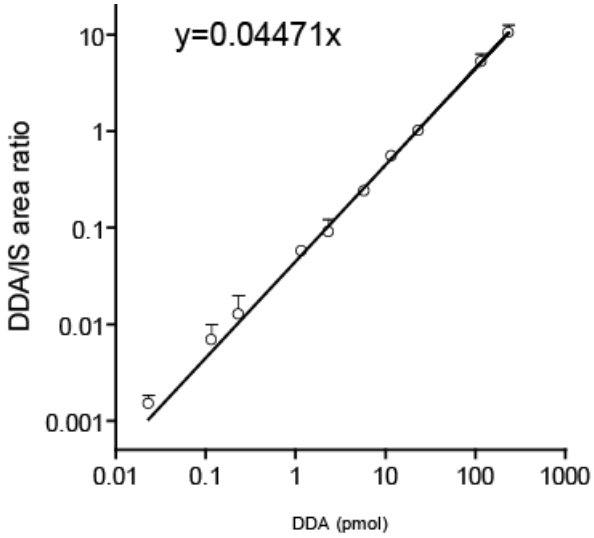

Supplementary Figure S4 | Calibration curve for quantification of DDA. MS^4 nanoESI mass spectrometry was used to determine *m/z* 424 (DDA) (Figure S2) over 431 (d7-DDA (Figure S5) used as internal standard (IS) ratios. Increasing concentrations of DDA were used with a constant IS concentration to obtain the calibration curve. The calibration curve was constructed using a quadratic regression with 1/x weighting that was linear in the concentration range of DDA. HPLC fractions excluding the 18-21 min HPLC fractions from mouse brain homogenates, which lack traces of DDA, were used as a quality control matrix. The 18-21 min HPLC fractions from tissue and cell homogenates containing d7-DDA were then submitted to nano-ESI analysis. Samples from three separate experiments were prepared and each sample was analyzed twice.

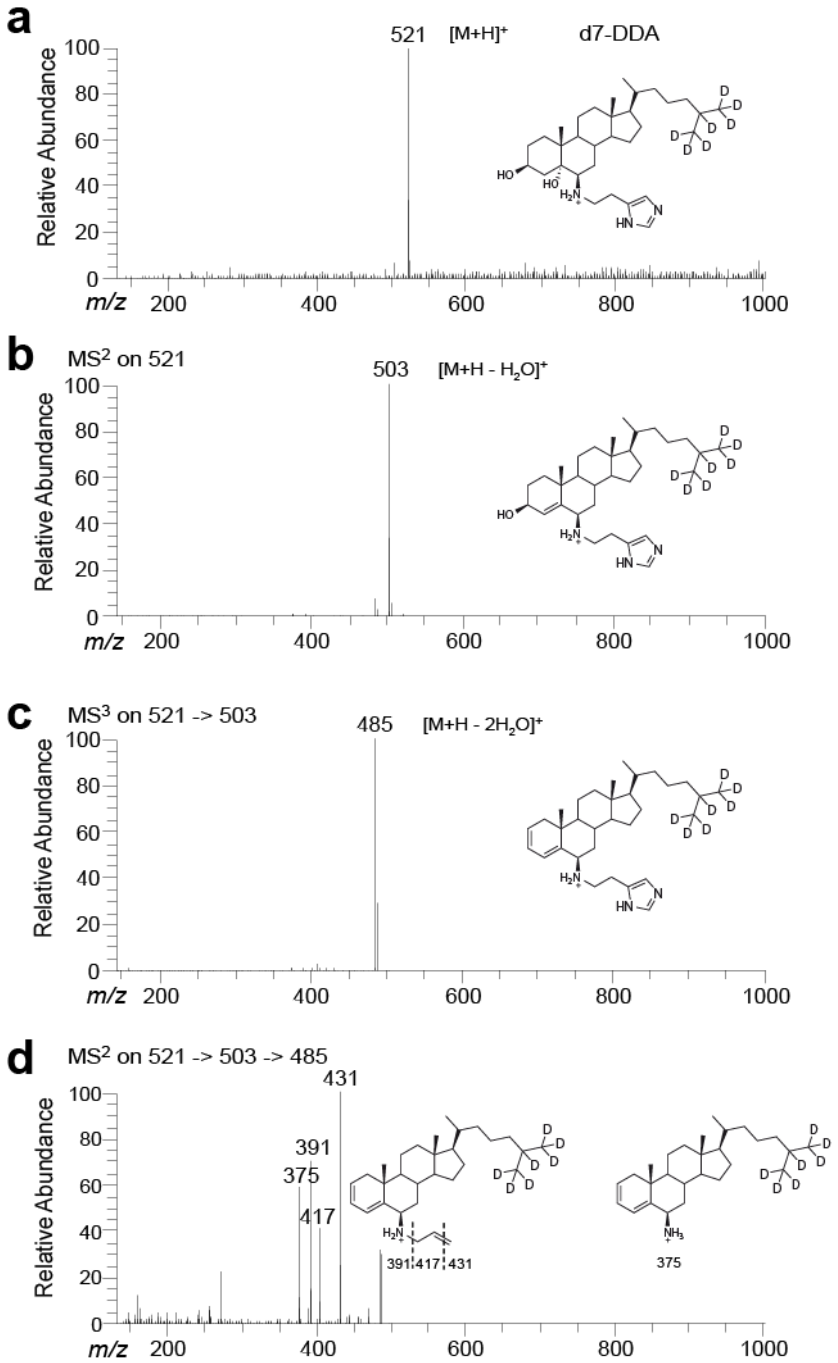

Supplementary Figure S5 | NanoESI fragmentation profiles of d7-DDA. (a) nanoESI Mass spectrometry fragmentation (MS^1) profile of d7-DDA and chemical structure of d7-DDA. (b) MS^2 fragmentation of the $[M+H]^+$ (*m/z* 521) peak obtained in MS^1. (c) MS^3 fragmentation of the (*m/z* 503) peak obtained in MS^2. (d) MS^4 fragmentation of the (*m/z* 485) peak obtained in MS^3.

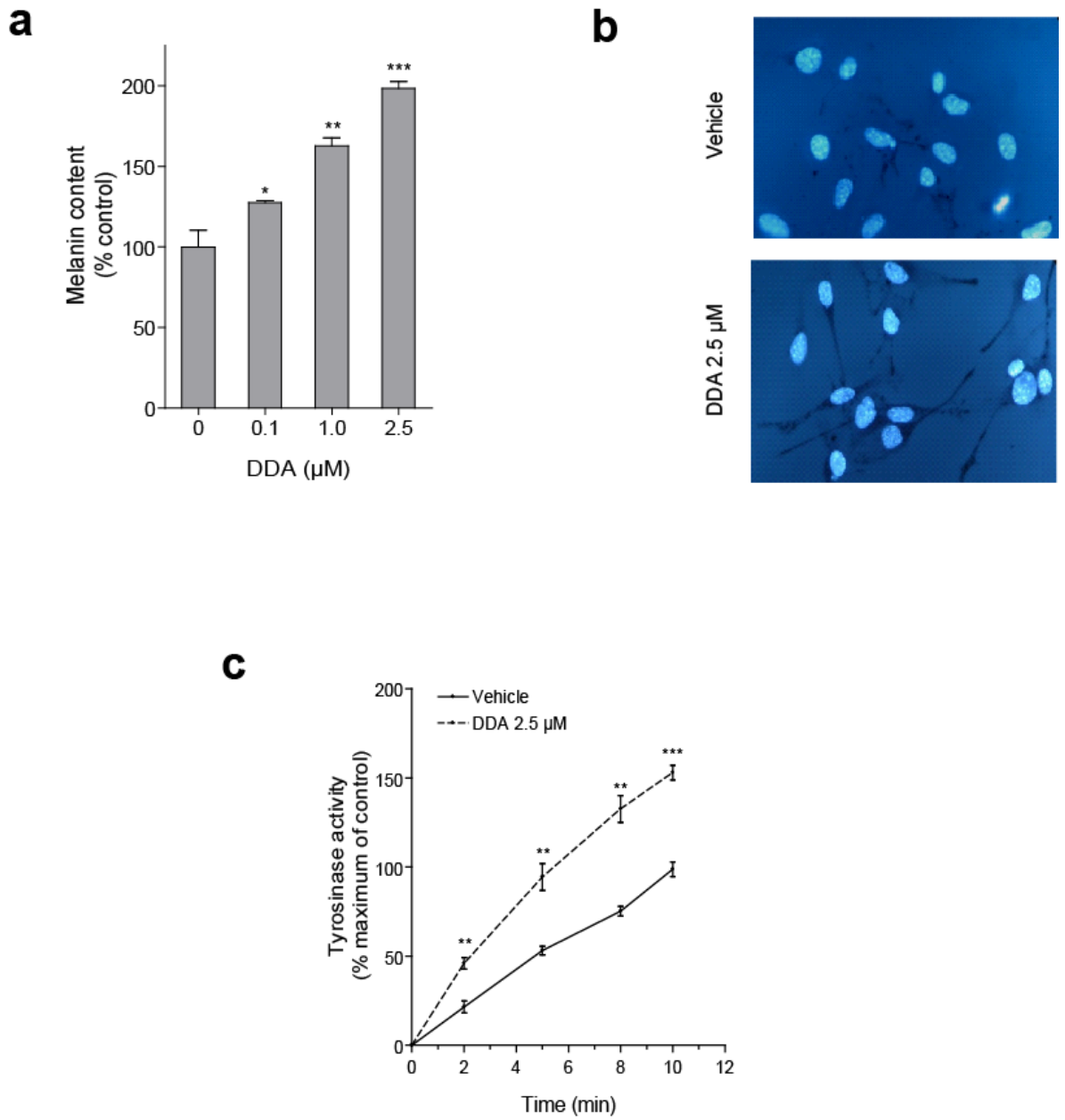

Supplementary Figure S6 | DDA induces B16F10 cell differentiation *in vitro*. Cells were treated for 24 h with solvent vehicle or the indicated concentrations of DDA. (a) DDA stimulated melanin biosynthesis in cells in a concentration-dependent manner and the appearance of melanin containing vesicles (b) and increased the tyrosinase activity (c). The melanin content is expressed as the percentage of the control. Pellets of 3.10^6 cells were used to measure the melanin content or tyrosinase activity spectrophotometrically. The tyrosinase activity was measured during the first 10 min, and a correction for auto-oxidation of L-DOPA was made using L-DOPA in the enzyme buffer in the absence of cell lysates. Results are the mean ± S.E.M. of three experiments performed in triplicate.

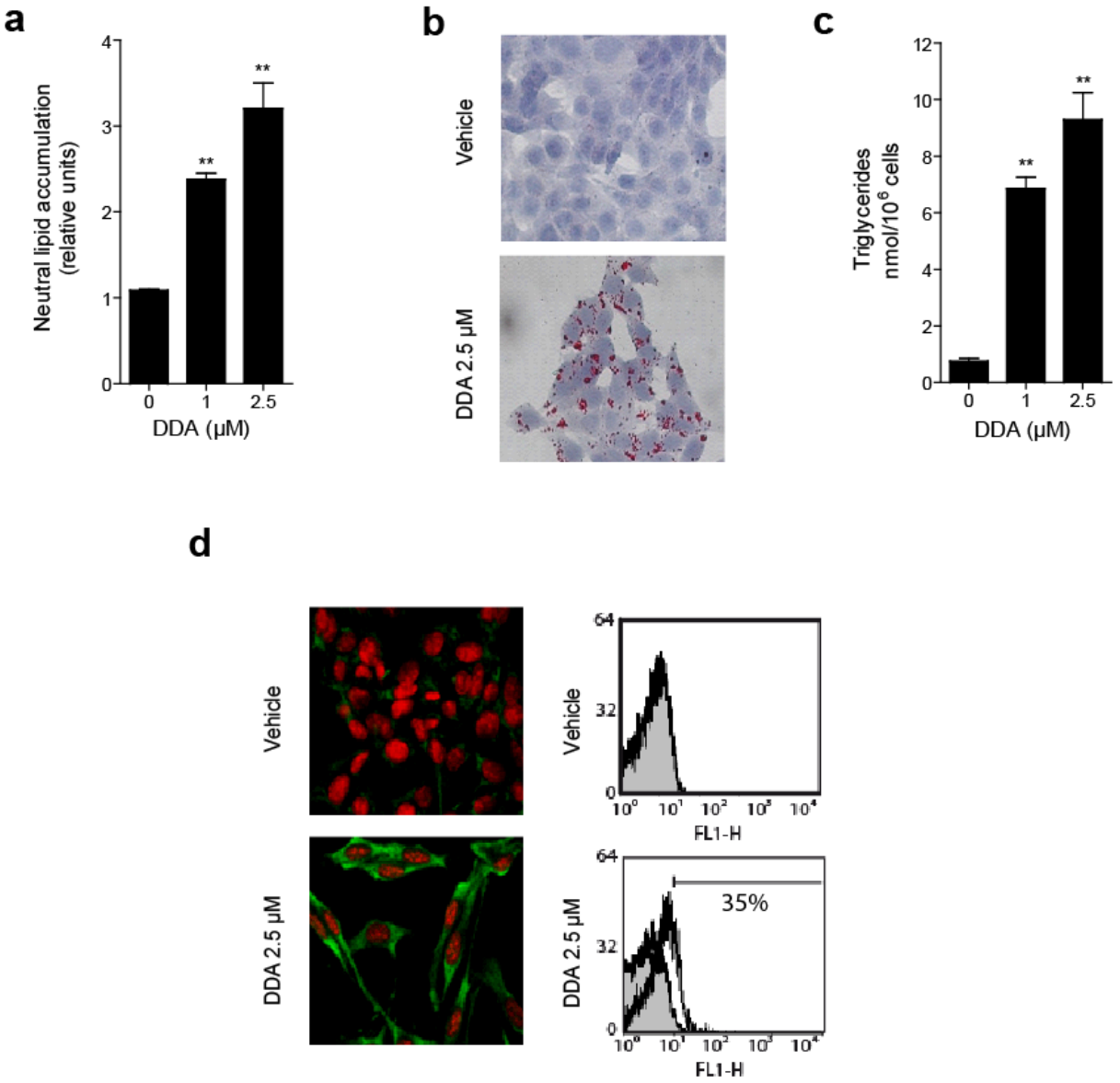

Supplementary Figure S7 | DDA induces TS/A cell differentiation *in vitro*. TS/A cells were treated for 24 h with the solvent vehicle or the indicated concentrations of DDA. Neutral lipids were stained with ORO and (a) quantified after extracting the ORO-stained cells by measuring the absorbance at 492 nm and (b) ORO-stained cells were observed with light microscopy (×25) after counterstaining with Mayer's hematoxylin. (c) triglycerides were quantified. (d) MFGE8 was analyzed by confocal fluorescence microscopy (×63) using an anti-MFGE8 antibody and a fluorescein-labeled anti-mouse secondary antibody and the nuclei were stained with propidium iodide (left panel). MFGE8 expression was quantified by flow cytometry with an anti-MFGE8 antibody (white peaks) or control isotype (grey peaks). Values indicated in the panel are the percentage of cells positive for the antibody relative to the isotype staining. Data are representative of three independent experiments.

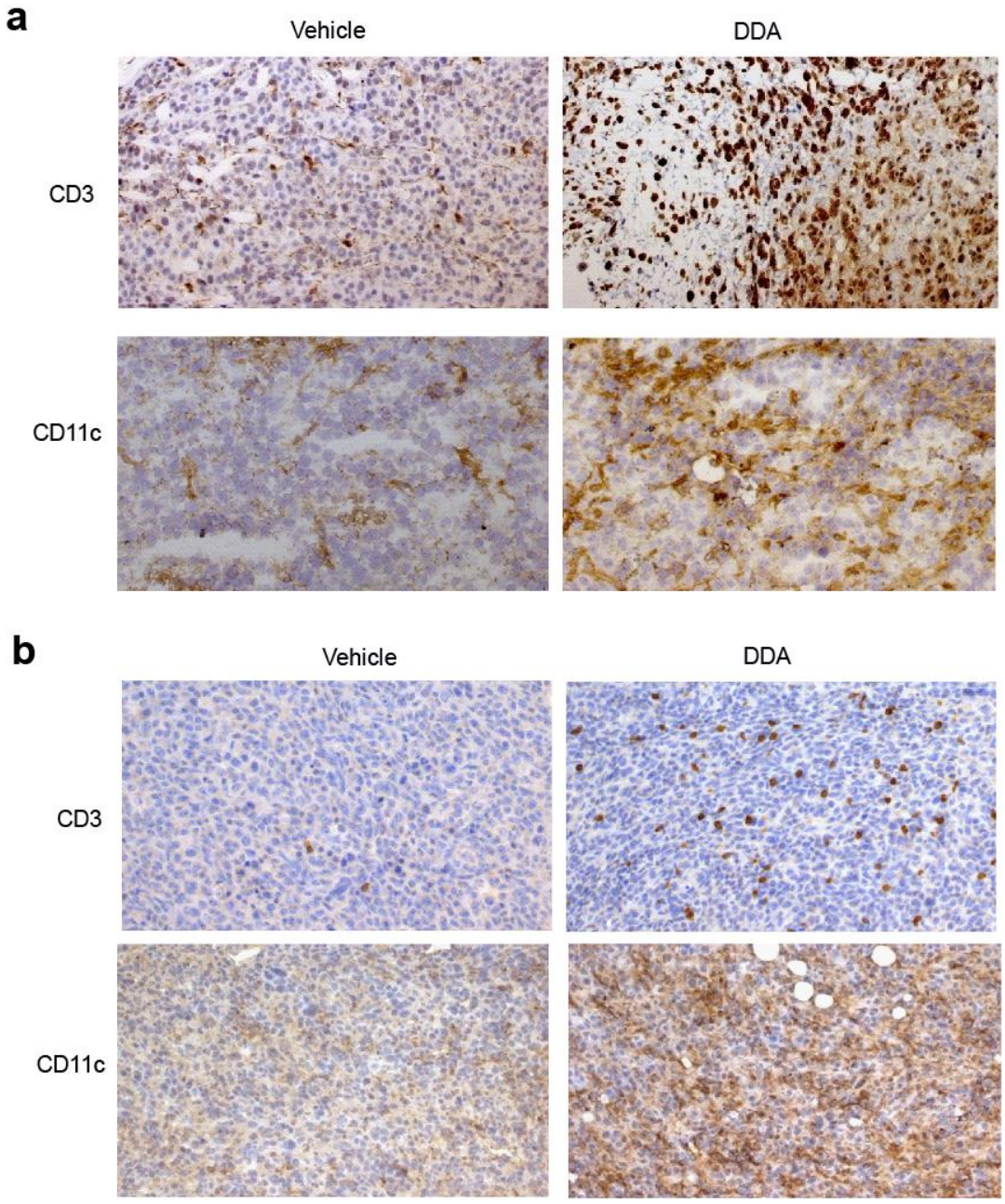

Supplementary Figure S8 | DDA induces intra-tumour immune cell infiltration in B16F10 and TS/A tumours implanted into immunocompetent mice. Histology of established tumours resected from immunocompetent mice treated with solvent vehicle (left panels) or DDA (3.7 µg/kg) (right panels). (a) B16F10 tumour sections from mice treated for 23 days and (b) TS/A tumours from mice treated for 30 days were analyzed for T lymphocytes (CD3) and DCs (CD11c) (brown staining) tumour infiltration. Paraffin-embedded tissue sections were incubated with the target retrieval solution S1700 (Dako) in a 95°C water bath for 40 min and then revealed using anti-CD3 antibodies to label T lymphocytes. anti-CD11c (1:25) that was used on frozen sections to label DCs in the cellular infiltrates. Following primary antibody incubation, sections were incubated with biotin-conjugated polyclonal secondary antibodies, followed by incubation with the avidin-biotin-peroxidase complex (Vectastain ABC kit, Vector Laboratories, CA). Diaminobenzidine (DAB) chromogen solution was used to visualize the signal, and the sections were then counter-stained with haematoxylin.

Supplementary Table S1 | Mass spectrometry fragmentation profile of the *m/z* 514 molecular ion of sDDA and synthetic C17.

	sDDA	sC17
m/z	Relative abundance (%)	
514	6.5	2.6
497		28.3
496	100	7.6
478	12.3	2.2
396	0.7	
385		49.5
368	1.5	
367		100
159		12.6

Supplementary Table S2 | Quantification of endogenous DDA in tumour cells. Quantification of DDA was done by nanoESI mass spectroscopy, by determining the under peak-area ratio of DDA (*m/z* 424) and d7-DDA (*m/z* 431) used as internal standard. These peaks were obtained on MS^4 spectra (Figure S2 and S4) and quantification was achieved according to the equation obtained from the calibration curve drawn on Figure S5. N.M.: not measurable. Studies were done with three different samples analyzed twice.

Cell line	Cell type	[DDA]
		ng/mg prot
A549	Lung carcinoma, human	N.M.
SK-N-SH	Neuroblastoma, human	N.M.
SH-SY5Y	Neuroblastoma, human	N.M.
Neuro2A	Neuroblastoma, mouse	N.M.
U87	Glioma, human	N.M.
GL261	Glioma, mouse	N.M.
U937	Monocyte leukemia, human	N.M.
NB4	Promyelocytic leukemia, human	N.M.
KG1	Acute myeloid leukemia, human	N.M.
HT29	Colon carcinoma, human	N.M.
HCT-8	Colon carcinoma, human	N.M.
SW 620	Intestinal carcinoma, human	N.M.

Supplementary Table S3 | Impact of DDA and C17 on mEH and sEH activity. Human sEH and rat mEH inhibition was tested by increasing concentrations of 1-trifluoromethoxyphe nyl-3-(1-propionylpiperidin-4-yl) urea (TFPPU), a selective inhibitor of sEH; 2-nonylsulfanyl-propionamide (2-NSP), a selective inhibitor of mEH; DDA and C17. The IC_{50} corresponds to the concentration required to inhibit 50 % of the enzyme activity as described in the "Methods" section.

Compound	sEH	mEH
	IC_{50} (μM)*	
TFPPU	0.004 ± 0.001	-
2-NSP	-	6.5 ± 0.8
DDA	> 100	> 100
C17	> 100	> 100

*Mean ± S.E.M. values (see Methods)